Fractal analysis of planar nilpotent singularities and numerical applications

Peer-reviewed author version

Horvat Dmitrovic, Lana; HUZAK, Renato; Vlah, Domagoj & Županovic´, Vesna
(2021) Fractal analysis of planar nilpotent singularities and numerical applications.
In: JOURNAL OF DIFFERENTIAL EQUATIONS, 293, p. 1-22.

DOI: 10.1016/j.jde.2021.05.015
Handle: http://hdl.handle.net/1942/34091

Fractal analysis of planar nilpotent singularities and numerical applications

Lana Horvat Dmitrović[1], Renato Huzak[2],

Domagoj Vlah[3] and Vesna Županović[4]

September 22, 2020

Abstract

The goal of our work is to give a complete fractal classification of planar analytic nilpotent singularities. For the classification, we use the notion of box dimension of (two-dimensional) orbits on separatrices generated by the unit time map. We also show how the box dimension of the one-dimensional orbit generated by the Poincaré map, defined on the characteristic curve near the nilpotent center/focus, reveals an upper bound for the number of limit cycles near the singularity. We introduce simple formulas for numerical calculation of the box dimension of one- and two-dimensional orbits and apply them to nilpotent singularities.

Keyword: nilpotent singularity, box dimension, unit-time map, Poincaré map, characteristic curve, numerical methods

Mathematical Subject Classification (2020): 34C07, 37C45, 37G10, 37M20

Address: [1], [3] and [4]: University of Zagreb, Faculty of Electrical Engineering and Computing, Department of Applied Mathematics, Unska 3, 10000 Zagreb, Croatia

[2]: Hasselt University, Campus Diepenbeek, Agoralaan Gebouw D, 3590 Diepenbeek, Belgium

1 Introduction

The connection between discrete and continuous dynamical systems has played an important role in bifurcation theory. One of the most commonly used connections is the connection via Poincaré map near the focus, limit cycle, homoclinic or heteroclinic loops and other polycycles. In [3], authors study the germs of diffeomorphisms in the plane by embedding them in the germ of an appropriate flow. The problem of embedding the diffeomorphism in the flow is solved by showing that a C^0 or C^r diffeomorphism is conjugated to the unit-time map of a flow of appropriate vector field. The reason for studying diffeomorphisms with this method is that the study of planar vector fields is generally easier than the study of planar diffeomorphisms. The unit-time map approach is also used to treat strong resonance cases in planar discrete dynamical systems (see e.g. [11]).

With our paper we pursue a twofold goal. Firstly, *we give a complete fractal classification of analytic nilpotent singularities in a two-dimensional setting* (the linear part of a nilpotent singularity is conjugated with $y\frac{\partial}{\partial x}$). Our fractal analysis is based on the notion of the box dimension of orbits generated by the unit-time map which tend to the (nilpotent) singularity along separatrices. On the other hand, *we numerically compute the box dimension of (two-dimensional) orbits along separatrices and of their (one-dimensional) projections.*

In [2] one finds all possible phase portraits of planar analytic nilpotent singularities (see also Theorem 1). One typically divides the nilpotent singularities into three cases (Hamiltonian like case, singular like case and mixed case) and blows up the singularity, where the chosen blow-up formula is depending on the case. Then one finds the type of singularity and detects all possible separatrices by means of the blown-up vector field (for more details see Section 2.1). As mentioned above, our focus is on the fractal analysis of the unit-time map along the separatrices (see Section 2), except for the center/focus type which has no separatrices and where we have to deal with the fractal analysis of the Poincaré map defined on the so-called characteristic curve (see Section 3). Note that in the C^∞-setting the same fractal analysis is also possible, except for the center/focus type and the nilpotent singularities with the multiplicity equal to ∞ (see Remark 1). In this paper, the multiplicity of a nilpotent singularity is denoted by m.

One of our motivations is that in some cases we can read the cyclicity (i.e. the maximum number of limit cycles) of a nilpotent singularity from the box dimension (see Section 3). We also note that in discrete dynamical systems the box dimension of orbits near a fixed point at the bifurcation point jumps from the trivial value (zero) to the corresponding value associated with the multiplicity of the fixed point and the type of bifurcation. In this way, the box dimension indicates the multiplicity, i.e. the maximum number of singularities that can bifurcate from the fixed point. Bifurcations of discrete systems related to the change of the box dimension of an orbit were studied in [7, 8, 13]. In the case of continuous systems, Hopf-Takens bifurcations have been studied using the box dimension of spiral trajectories of normal forms and of orbits generated by the Poincaré map in [20, 22]. According to [7, 8], the change in box dimension can be seen in the unit-time map of one-dimensional or planar semi-hyperbolic continuous systems. The remaining cases in the (continuous) planar setting are

nilpotent and more degenerate singularities. In our paper we concentrate on the fractal analysis of the nilpotent singularities.

In [12] there is a new method to study the cyclicity of the nilpotent focus by means of a generalised polar coordinate transformation. The Poincaré successor function and the Lyapunov constants give the upper bound for the number of limit cycles. In [6] it has been proved that the upper bound for the cyclicity of the nilpotent focus is directly related to the first non-zero Lyapunov constant of the projection on the x-axis of the Poincaré map defined on the characteristic curve.

In our work we connect the result from [6] with the box dimension of any orbit of the Poincaré map on the characteristic curve and obtain a simple sufficient condition (expressed in terms of the box dimension) for the upper bound for the cyclicity of the nilpotent focus.

Since the box dimension is defined for bounded sets, we investigate sequences (orbits) of points that have a limit at singular point (origin). So we are interested in the trajectories that contain the origin. Sometimes we deal with the box dimension of a map instead of an orbit (e.g. the box dimension of the unit-time map, etc.) It is equal to the box dimension of any orbit (on a fixed separatrix) generated by the map. The box dimension will be independent of the selected orbit (for more details see Section 2.3).

The box dimension was defined using the leading term of asymptotic expansion of the volume of the ε-neighborhood of a set. Considering some other terms, more properties of the considered dynamical system can be obtained. Normal forms of parabolic diffeomorphisms were considered in [15, 16] using the fractal approach. Formal embeddings of Dulac maps in flows of vector fields in the one-dimensional case were investigated in [14]. More about applications of fractal dimensions in dynamical systems can be found in [21].

Now we recall the concept of the box dimension. For further details see for example [5, 19]. Let $A \subset \mathbb{R}^N$ be bounded. The ε-neighborhood of A is defined by $A_\varepsilon = \{y \in \mathbb{R}^N : d(y, A) \leq \varepsilon\}$. Let $s \geq 0$. *The lower and upper s-dimensional Minkowski contents of A* are defined by

$$\mathcal{M}_*^s(A) := \liminf_{\varepsilon \to 0} \frac{|A_\varepsilon|}{\varepsilon^{N-s}}, \quad \mathcal{M}^{*s}(A) := \limsup_{\varepsilon \to 0} \frac{|A_\varepsilon|}{\varepsilon^{N-s}}$$

where $|A_\varepsilon|$ is the Lebesgue measure of A_ε. Then *the lower and upper box dimension* are given by

$$\underline{\dim}_B A = \inf\{s \geq 0 : \mathcal{M}_*^s(A) = 0\}, \quad \overline{\dim}_B A = \inf\{s \geq 0 : \mathcal{M}^{*s}(A) = 0\}.$$

If $\underline{\dim}_B A = \overline{\dim}_B A$ we denote it by $\dim_B A$. If $\Psi : A \subset \mathbb{R}^N \to \mathbb{R}^M$ is a Lipschitz map, then

$$\underline{\dim}_B \Psi(A) \leq \underline{\dim}_B A, \ \overline{\dim}_B \Psi(A) \leq \overline{\dim}_B A.$$

We say that $\Psi : A \subset \mathbb{R}^N \to \mathbb{R}^M$ is a bi-Lipschitz map if there exist positive constants a_1 and a_2 such that

$$a_1 \|x - y\| \leq \|\Psi(x) - \Psi(y)\| \leq a_2 \|x - y\|,$$

for every $x, y \in A$. If Ψ is a bi-Lipschitz map, then

$$\underline{\dim}_B A = \underline{\dim}_B \Psi(A), \ \overline{\dim}_B A = \overline{\dim}_B \Psi(A).$$

We say that two sequences $(x_k)_{k\geq 1}$ and $(y_k)_{k\geq 1}$ of positive real numbers are *comparable* and write $x_k \simeq y_k$ as $k \to \infty$ if $a_1 \leq x_k/y_k \leq a_2$ for some $a_1, a_2 > 0$ and all $k \geq 1$. Analogously, two positive functions $f, g : (0, r) \to \mathbb{R}$ are comparable and we write $f(x) \simeq g(x)$ as $x \to 0$ if $f(x)/g(x) \in [a_1, a_2]$ for x small enough. If $|A_\varepsilon| \simeq \varepsilon^s$ as $\varepsilon \to 0$, then $\dim_B A = N - s$.

In Section 2 we concentrate on the fractal analysis of the unit-time map in the vicinity of nilpotent singularities with separatrices. We also prove a general result about the box dimension of two-dimensional (and higher dimensional) discrete dynamical systems. Section 3 is dedicated to the nilpotent focus. Theorem 4 shows how the upper bound for cyclicity can be found from the box dimension of the Poincaré map on the characteristic curve. In Section 4 the fractal analysis of Bogdanov-Takens bifurcations is given. In Section 5 we numerically calculate the box dimension of orbits on the separatrices.

2 Fractal analysis of nilpotent singularities and the unit-time map

2.1 Nilpotent singularities and separatrices

First we recall the well-known theorem about the classification of analytic nilpotent singularities for planar vector fields (see [2]).

Theorem 1. [2] (**Nilpotent Singular Points**) *Let* $(0, 0)$ *be a singular point of the vector field given by*

$$\begin{aligned} \dot{x} &= y + H_1(x, y), \\ \dot{y} &= H_2(x, y), \end{aligned} \tag{1}$$

where H_1 *and* H_2 *are analytic functions in a neighborhood of the point* $(0, 0)$ *and* $j_1 H_1(0, 0) = j_1 H_2(0, 0) = 0$. *Let* $y = f(x)$ *be the characteristic curve of (1), i.e. the solution of the equation* $y + H_1(x, y) = 0$ *in a neighborhood of the point* $(0, 0)$ *and consider* $F(x) = H_2(x, f(x))$ *and* $G(x) = (\frac{\partial H_1}{\partial x} + \frac{\partial H_2}{\partial y})(x, f(x))$. *Then the following holds:*
(1) If $F(x) \equiv G(x) \equiv 0$, *then (1) has the curve of singularities* $y = f(x)$ *passing through the origin (see Figure 1(a)).*
(2) If $F(x) \equiv 0$ *and* $G(x) = bx^n + o(x^n)$ *for* $n \in \mathbb{N}$, $n \geq 1$, $b \neq 0$, *then (1) has the curve of singularities* $y = f(x)$ *passing through the origin (Figure 1(b1) or (b2)).*
(3) If $G(x) \equiv 0$ *and* $F(x) = ax^m + o(x^m)$ *for* $m \in \mathbb{N}$, $m \geq 2$, $a \neq 0$, *then*
(i) If m *is odd and* $a > 0$, *then the origin is a saddle (Figure 1(d)); and if* $a < 0$, *then it is a center or a focus (Figure 1(h1)–(i));*
(ii) If m *is even, then the origin is a cusp (Figure 1(c)).*
(4) If $F(x) = ax^m + o(x^m)$ *and* $G(x) = bx^n + o(x^n)$, $m, n \in \mathbb{N}$, $m \geq 2$, $n \geq 1$, $a \neq 0$, $b \neq 0$, *then we have:*
(i) If m *is even, and*
(i1) $m < 2n + 1$, *then the origin is a cusp (Figure 1(c));*
(i2) $m > 2n + 1$, *then the origin is a saddle-node (Figure 1(e1) or (e2)).*
(ii) If m *is odd and* $a > 0$, *then the origin is a saddle (Figure 1(d)).*

(iii) If m is odd, $a < 0$ and
(iii1) Either $m < 2n+1$, or $m = 2n+1$ and $b^2 + 4a(n+1) < 0$, then the origin is a center or a focus (Figure 1(h1)–(i));
(iii2) n is odd and either $m > 2n+1$, or $m = 2n+1$ and $b^2 + 4a(n+1) \geq 0$, then the phase portrait of the origin consists of one hyperbolic and one elliptic sector (Figure 1(g));
(iii3) n is even and $m > 2n+1$ or $m = 2n+1$ and $b^2 + 4a(n+1) \geq 0$, then the origin is a node (repelling if $b > 0$ and attracting if $b < 0$). See Figure 1(f1) or (f2).

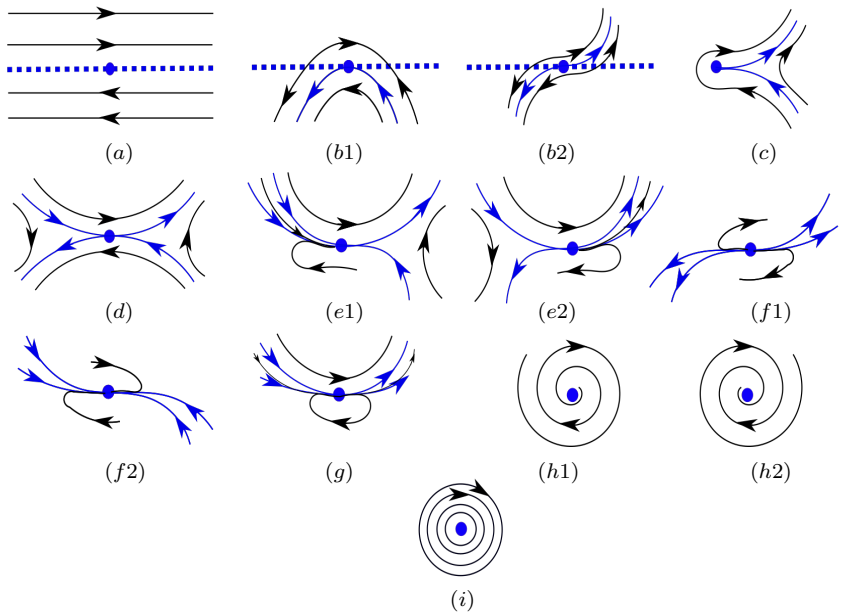

Figure 1: Phase portraits of nilpotent singularities with indication of separatrices, colored blue.

For the sake of readability, we list the results of Theorem 1 in Table 1. To prove Theorem 1, system (1) near the origin first has to be brought into a normal form (4) (i.e. (5)) for C^∞-conjugacy. Then one can easily blow up the origin in the normal form coordinates. One distinguishes between three cases: Hamiltonian like case ($m < 2n+1$), singular like case ($m > 2n+1$) and mixed case ($m = 2n+1$). In each of these cases a quasihomogeneous blow-up has been used to desingularize the system near the origin. When $m < 2n+1$ (including $n = \infty$) and m is odd (resp. even), one uses $(x, y) = (u\bar{x}, u^{\frac{m+1}{2}}\bar{y})$ (resp. $(x, y) = (u^2\bar{x}, u^{m+1}\bar{y})$). If $m > 2n+1$ (including $m = \infty$) or $m = 2n+1$, then the blow-up is given by $(x, y) = (u\bar{x}, u^{n+1}\bar{y})$. For each case the system has been studied in different charts ($\bar{x} = \pm 1$, $\bar{y} = \pm 1$) and one ends up with the types of nilpotent singularities listed in Table 1. It suffices to deal with the charts $\bar{x} = \pm 1$ (one finds no extra singularities in the charts $\bar{y} = \pm 1$). For more details see Section 3.4 in [2].

The main advantage of the above blow-up is that in the blow-up coordinates

(after division by some u^α) one has hyperbolic and semi-hyperbolic singularities the dynamics of which can be easily studied using the stable/unstable and center manifold theorem, etc. This way one detects all possible separatrices which are given in Table 1 (in the blow-down (x, y)-coordinates). The separatrices are invariant and contain the origin and our goal is to study the box dimension of the orbits on the separatrices generated by the unit-time map and tending to the origin. *We give a complete fractal classification for analytic nilpotent singularities* (for more details about the fractal classification of C^∞-nilpotent singularities see Remark 1).

In Hamiltonian like case (including $n = \infty$) saddle and cusp have each two separatrices with the leading order $\frac{m+1}{2}$, generated by hyperbolic saddles $\bar{y} \neq 0$ in the charts $\bar{x} = \pm 1$. Note that the center/focus type has no separatrices (its fractal analysis is given in Section 3 using a different approach). In singular like case with $m < \infty$ each type has two separatrices with different leading orders. The separatrix of order $n + 1$ originates from a hyperbolic saddle at $\bar{y} \neq 0$ detected in the charts $\bar{x} = \pm 1$ while a separatrix with the leading order $m - n$ comes from a semi-hyperbolic singularity $\bar{y} = 0$ in the same charts with $\{u = 0\}$ as the stable/unstable manifold and a center manifold transverse to it (in fact the separatrix comes from a center manifold $\bar{y} = \rho(u)$ with u^{m-2n-1} as the leading term in ρ). The case $m = \infty$ has one separatrix with order $n + 1$, as above, and a curve of singularities (the existence of the curve of singularities follows from the analyticity of (1)). For example, the system $\{\dot{x} = y, \dot{y} = -xy\}$ has the separatrix $y = -\frac{1}{2}x^2$ containing the origin and the curve of singularities $\{y = 0\}$. The fractal analysis of a *perturbation* of such system can be found in [1] (one uses singular perturbation theory). In mixed case one has two separatrices of leading order $n + 1$ (both of them come from hyperbolic singularities $\bar{y} \neq 0$) except for the case with $\Delta = 0$ where one deals with a separatrix of order $n+1$ coming from a semi-hyperbolic singularity at $\bar{y} \neq 0$ in $\bar{x} = \pm 1$ with stable/unstable manifold transverse to $\{u = 0\}$. The center/focus has no separatrices (see Section 3). When $m = n = \infty$, one has a curve of singularities and no separatrices (a typical example is $\{\dot{x} = y, \dot{y} = 0\}$.) Here, one uses again the analyticity of (1). See [2].

We point out that each separatrix has the form $y = \alpha x^\gamma + o(x^\gamma)$ with $\alpha \neq 0$ and $\gamma \in]1, m[$ (when we need smoothness property of the $o(x^\gamma)$-term, we mention it explicitly).

Remark 1. *If system (1) is (C^∞-) smooth, then we can use the same normal form (4) for C^∞-conjugacy and the same blow-up as before (see Section 3.4 in [2]). We end up with the same fractal classification as in the analytic case as long as m is kept finite and the singularity is not of center/focus type. When $m = \infty$, we don't know the type of nilpotent singularity (not necessarily non-isolated singularity like in the analytic case) but nevertheless we can give a partial fractal analysis. More precisely, when $m = \infty$ and n is finite, we detect a separatrix of order $n+1$ in the chart $\bar{x} = \pm 1$ as given in Table 1 with the same box dimensions. The center behavior $\bar{y} = \rho(u)$ at semi-hyperbolic singularity $\bar{y} = 0$ in the same charts is flat. We therefore cannot find the dynamics and the box dimension along center manifolds. We don't treat the case $m = n = \infty$ in the C^∞ setting. We also don't treat the center/focus type.*

In Section 2.2 we find the Taylor expansion of the unit-time map at the origin working with (5). In Section 2.3 we give a complete fractal study of

$m \geq 2, n \geq 1$		$a, b \neq 0$	type	separatrices	box dim.
Hamiltonian case $m < 2n+1$	m odd	$a > 0$	saddle	$y = \pm\sqrt{\frac{2a}{m+1}}\, x^{\frac{m+1}{2}} + \dots$	$(\frac{m-1}{m+1}, \frac{m-1}{m+1}, \frac{m-1}{2m})$
		$a < 0$	center/focus	–	–
	m even	$a > 0$	cusp	$y = \pm\sqrt{\frac{2a}{m+1}}\, x^{\frac{m+1}{2}} + \dots,\ x > 0$	$(\frac{m-1}{m+1}, \frac{m-1}{m+1}, \frac{m-1}{2m})$
		$a < 0$	cusp	$y = \pm\sqrt{\frac{-2a}{m+1}}(-x)^{\frac{m+1}{2}} + \dots,\ x < 0$	$(\frac{m-1}{m+1}, \frac{m-1}{m+1}, \frac{m-1}{2m})$
Singular case $m > 2n+1$	m odd	$a > 0$	saddle	$y = \frac{b}{n+1} x^{n+1} + \dots$	$(\frac{n}{n+1}, \frac{n}{n+1}, \frac{n}{2n+1})$ $(\frac{m-n-1}{m-n}, \frac{m-n-1}{m-n}, \frac{m-n-1}{2m-2n-1})$
		$a < 0$, n odd	elliptic		
		$a < 0$, n even	node	$y = -\frac{a}{b} x^{m-n} + \dots$	
	m even	–	saddle-node		
	$m = \infty$	–	curve of sing.	$y = \frac{b}{n+1} x^{n+1} + \dots$	$(\frac{n}{n+1}, \frac{n}{n+1}, \frac{n}{2n+1})$
Mixed case $m = 2n+1$	–	$a > 0$	saddle	$y = \frac{b \pm \sqrt{\Delta}}{2(n+1)} x^{n+1} + \dots$	$(\frac{n}{n+1}, \frac{n}{n+1}, \frac{n}{2n+1})$
	n odd	$a < 0, \Delta \geq 0$	elliptic		
	n even	$a < 0, \Delta \geq 0$	node		
	–	$a < 0, \Delta < 0$	center/focus	–	–
$m = n = \infty$	–	–	curve of sing.	–	–

Table 1: The classification of analytic nilpotent singularities w.r.t. the box dimension of the unit-time map of the normal form (5) of (1) for C^∞-conjugacy, along separatrices of (5). Each vector in the last column has three components. The first component is the box dimension of (any) two dimensional orbit S on separatrix generated by the unit-time map in forward or backward time. The second (resp. third) component is the box dimension of the one-dimensional orbit A (resp. B) consisting of the x-components (resp. y-components) of S. The box dimensions come from Theorem 2. We write $\Delta = b^2 + 4a(n+1)$. The Hamiltonian like case includes $n = \infty$.

(analytic) nilpotent singularities (5) (excluding center/focus) using the box dimension approach. The results obtained in Section 2.3 (see Theorem 2) are given in the last column of Table 1. For each separatrix, we find the vector $(\dim_B S, \dim_B A, \dim_B B)$ where S is a two-dimensional orbit on the separatrix generated by the unit-time map of (5) and where A and B are projections onto the x-axis and y-axis respectively. The box dimension of S (resp. A and B) is computed in two-dimensional (resp. one-dimensional) ambient space. It will be clear from Section 2.3 that the above box dimensions are well-defined, i.e. independent of the initial point of S on the fixed separatrix.

Since a C^∞-coordinate change is a bi-Lipschitz map, the box dimension of orbits on a separatrix is preserved under C^∞-conjugacy (i.e. (5) and (1) have the same box dimension along the separatrices).

To find the box dimensions (i.e., to prove Theorem 2 in Section 2.3) it is natural to distinguish between the three cases explained above. As we pass through different regions in the (m, n)-space we see that the leading property of the terms ax^m and $bx^n y$, along separatrices, changes. When $m < 2n+1$, the term ax^m is dominant and when $m > 2n+1$ the term bx^n becomes dominant ($\gamma = m - n$ is an exception). On the line $m = 2n+1$, the terms have the same order along the separatrices. In the proof of Theorem 2 we see that only the first term in the expansion of the separatrices (the term is given in Table 1) is sufficient to conclude about the box dimensions.

Note that, for a fixed nilpotent singularity, two separatrices (if they exist) with the same order but different coefficients in front of the leading term have

the same box dimension. Note also that we have the following properties of the box dimensions from Table 1: $\dim_B A > \dim_B B$ and $\dim_B S = \dim_B A$. The former follows from the fact that $\gamma > 1$ for all separatrices and that the box dimension measures the density of a sequence (the bigger the box dimension of the sequence, the higher the density of the sequence). The y-projection tends faster to 0 than the x-projection and its density is therefore lower. The latter is then a simple consequence of Lemma 2. We conclude this section by pointing out that in the singular like case the box dimensions attached to $\gamma = n + 1$ are smaller than the box dimensions attached to $\gamma = m - n$. This follows from the fact that a separatrix with $\gamma = m - n$ is a center manifold in the blow-up coordinates (i.e. the hyperbolicity is lost). As a consequence of this, the convergence to the origin of the unit-time map orbits is slower, and the box dimension is therefore bigger (see e.g. [4] for more details). This is the reason why the computation of the box dimension of orbits on separatrices with $\gamma = m - n$ may be more difficult from the numerical point of view (see Section 5).

2.2 Unit-time map of nilpotent singularities

We consider a continuous dynamical system

$$\dot{\mathbf{x}} = \mathbf{F}(\mathbf{x}) \tag{2}$$

where $\mathbf{x} \in \mathbb{R}^N$, $\mathbf{F} : \mathbb{R}^N \to \mathbb{R}^N$. The simplest way of getting a discrete dynamical system from the continuous one is by using flow for fixed t, $\phi_t(\mathbf{x})$. Namely, we fix $t_0 > 0$ and we consider the system which is generated by the iteration of the map ϕ_{t_0} (map with displacement t_0 along the trajectory of (2)). If we take $t_0 = 1$, we get the unit-time map $\phi_1(\mathbf{x})$ and we can study the discrete dynamical system generated by the unit-time map

$$\mathbf{x} \mapsto \phi_1(\mathbf{x}). \tag{3}$$

Suppose $\mathbf{x_0} = 0$ is a singularity of (2). Then $\mathbf{F}$ can be written as

$$\mathbf{F}(\mathbf{x}) = A\mathbf{x} + \mathbf{F}^{(2)}(\mathbf{x}) + \mathbf{F}^{(3)}(\mathbf{x}) + \dots, \;\; \mathbf{x} \in \mathbb{R}^N,$$

where $A = D\mathbf{F}(0)$ and $\mathbf{F}^{(k)}$ is a polynomial vector function of order k with

$$F_i^{(k)}(\mathbf{x}) = \sum_{j_1+\dots+j_n=k} b_{i,j_1,\dots,j_n} x_1^{j_1} x_2^{j_2} \dots x_n^{j_n}.$$

Our goal is to find the Taylor expansion of $\phi_t(\mathbf{x})$ near $\mathbf{x_0} = 0$ by using the process of Picard iterations (see e.g. [11]). Namely, let $\mathbf{x}^{(1)}(t) = e^{At}\mathbf{x}$ be a solution of linear equation $\dot{\mathbf{x}} = A\mathbf{x}$ with the initial value $\mathbf{x}$, and define

$$\mathbf{x}^{(k+1)}(t) = e^{At}\mathbf{x} + \int_0^t e^{A(t-\tau)} \left(\mathbf{F}^{(2)}(\mathbf{x}^{(k)}(\tau)) + \dots + \mathbf{F}^{(k+1)}(\mathbf{x}^{(k)}(\tau)) \right) d\tau.$$

It can be easily seen that the $(k+1)$-iteration does not change the terms of order $l \leq k$. By the substitution $t = 1$ in $\mathbf{x}^{(k)}(t)$ we get the (exact) Taylor expansion of the unit-time map (3) up to the terms of order $\leq k$

$$\phi_1(\mathbf{x}) = e^A\mathbf{x} + \mathbf{g}^{(2)}(\mathbf{x}) + \dots + \mathbf{g}^{(k)}(\mathbf{x}) + \dots,$$

where $\mathbf{g}^{(i)}$ are polynomial vector functions of a form as functions $\mathbf{F}^{(i)}$.

In this section we compute the Taylor expansion of the unit-time map of normal form (5) of (1) at $(x, y) = (0, 0)$. Following Section 3.4 in [2] we have the following normal form of (1) for C^∞-conjugacy:

$$\begin{aligned} \dot{x} &= y \\ \dot{y} &= F(x) + yG(x) + y^2 H(x, y), \end{aligned} \tag{4}$$

where F, G and H are C^∞-functions, $j_1 F(0) = G(0) = j_\infty H(0, 0) = 0$. We write $F(x) = ax^m + o(x^m)$ and $G(x) = bx^n + o(x^n)$ with $a \neq 0$, $b \neq 0$, $m \geq 2$ and $n \geq 1$. In the case $j_\infty F(0) = 0$ (resp. $j_\infty G(0) = 0$) we take $m = \infty$ (resp. $n = \infty$). System (4) can be written as

$$\begin{aligned} \dot{x} &= y \\ \dot{y} &= ax^m + bx^n y + y^2 H(x, y) + \mathcal{O}(x^{m+1}) + y\mathcal{O}(x^{n+1}). \end{aligned} \tag{5}$$

Remark 2. *We point out that there exists an analytic coordinate change bringing (1) near the origin to (4) with some analytic functions F and G and $H \equiv 0$ (see [17]). Since in our paper the analytic normal form (with $H \equiv 0$) does not simplify the computations, we prefer to work with the smooth normal form (5).*

Using the Picard iterations we prove the following lemma about the Taylor expansion of the unit-time map of (5) depending on the region in the (m, n)-space.

Lemma 1. (**The unit-time map**)
Let the origin be a nilpotent singularity of the system (5)*. Then the following holds for the orbit $\{(x_k, y_k)\}_{k\in\mathbb{N}}$ with the initial point (x_0, y_0) generated by the unit-time map of* (5)*:*

1. *If $m < n + 1$, then*

$$\begin{aligned} x_{k+1} &= x_k + y_k + \frac{a}{2}x_k^m + ac_{11}x_k^{m-1}y_k + \ldots + ac_{1m}y_k^m + h.o.t. \\ y_{k+1} &= y_k + ax_k^m + ad_{11}x_k^{m-1}y_k + \ldots + ad_{1m}y_k^m + h.o.t.; \end{aligned} \tag{6}$$

   with constants $c_{1i} = c_{1i}(m)$, $d_{1i} = d_{1i}(m)$.

2. *If $m = n + 1$, then*

$$\begin{aligned} x_{k+1} &= x_k + y_k + \frac{a}{2}x_k^m + c_{21}x_k^{m-1}y_k + \ldots + c_{2,m-1}x_k y_k^{m-1} + c_{2,m}y_k^m + h.o.t. \\ y_{k+1} &= y_k + ax_k^m + d_{21}x_k^{m-1}y_k + \ldots + d_{2m}y_k^m + h.o.t.; \end{aligned} \tag{7}$$

   with constants $c_{2i} = c_{2i}(m, a, b)$, $d_{2i} = d_{2i}(m, a, b)$.

3. *If $m > n + 1$, then*

$$\begin{aligned} x_{k+1} &= x_k + y_k + \frac{b}{2}x_k^n y_k + bc_{31}x_k^{n-1}y_k^2 + \ldots + bc_{3,n-1}x_k y_k^n + \frac{by_k^{n+1}}{n+2} + h.o.t. \\ y_{k+1} &= y_k + bx_k^n y_k + bd_{31}x_k^{n-1}y_k^2 + \ldots + bd_{3,n-1}x_k y_k^n + \frac{by_k^{n+1}}{n+1} \\ &\quad + \cdots + ax_k^m + \ldots; \end{aligned} \tag{8}$$

   with constants $c_{3i} = c_{3i}(n)$, $d_{3i} = d_{3i}(n)$, $i = 1, \ldots, n-1$ where the x_k^i-terms occur in the above expansion only if $i \geq m$.

Proof. In the case $m \leq n+1$, by using the Picard iterations we find the Taylor expansion of the unit-time map up to terms of order m. If $m < n+1$ (resp. $m = n+1$), the terms of order m in (6) (resp. (7)) are generated by the term ax^m (resp. $ax^m + bx^n y$) in (5). When $m > n+1$ we easily get the Taylor expansion up to terms of order $n+1$ (the terms of order $n+1$ are generated by the term $bx^n y$ in (5)) and compute the coefficient in front of x^m. □

Remark 3. *Note that the case where $m = \infty$ (resp. $n = \infty$) is included in Lemma 1.3 (resp. Lemma 1.1). The case where $m = n = \infty$ occurs in Theorem 1(1) and the fractal analysis of the corresponding (non-isolated) nilpotent singularity is not needed, as explained in Section 2.1.*

2.3 The box dimension of orbits on separatrices

In this section we prove a result for the box dimension of the unit-time map of (5) on a (fixed) separatrix introduced in Section 2.1. We define it as the box dimension of any orbit on the separatrix generated by the unit-time map and tending to the origin (see Theorem 2). This box dimension is well-defined, i.e. independent of the chosen orbit, or equivalently, of the initial point (x_0, y_0) on the separatrix. This will follow directly from Lemma 2 and the fact that the box dimension of one-dimensional discrete orbit is independent of the initial point (see e.g. Theorem 1 in [4] or Theorem 1 in [13]). First we prove the following lemma about the box dimension of two-dimensional sequences.

Lemma 2. (Box dimension of two-dimensional discrete orbit)
Let $A = \{x_k\}_{k\in\mathbb{N}}$ and $B = \{y_k\}_{k\in\mathbb{N}}$ be two decreasing sequences which tend to 0 with initial points x_0 and y_0 and with the properties $x_k - x_{k+1} \simeq x_k^\alpha$, for $\alpha > 1$ and $y_k - y_{k+1} \simeq y_k^\beta$, for $\beta > 1$, as $k \to \infty$. Moreover, let $(x_k - x_{k+1})_{k\in\mathbb{N}}$ and $(y_k - y_{k+1})_{k\in\mathbb{N}}$ be monotonically nonincreasing. Let $S = \{(x_k, y_k)\}_{k\in\mathbb{N}}$ be the orbit defined using A and B. If $\alpha \geq \beta$ (resp. $\alpha < \beta$), then $\dim_B S = \dim_B A = 1 - \frac{1}{\alpha}$ (resp. $\dim_B S = \dim_B B = 1 - \frac{1}{\beta}$).

Proof. Since $\alpha, \beta > 1$, Theorem 1 in [4] implies that $\dim_B A = 1 - \frac{1}{\alpha}$, $\dim_B B = 1 - \frac{1}{\beta}$, $x_k \simeq k^{-\frac{1}{\alpha-1}}$ and $y_k \simeq k^{-\frac{1}{\beta-1}}$ as $k \to \infty$. In the rest of the proof we assume that $\alpha \geq \beta$ (the case where $\alpha < \beta$ can be proved in a similar way). We have

$$a_1 k^{-\frac{\alpha}{\alpha-1}} \leq x_k - x_{k+1} \leq a_2 k^{-\frac{\alpha}{\alpha-1}} \quad \text{and} \quad b_1 k^{-\frac{\beta}{\beta-1}} \leq y_k - y_{k+1} \leq b_2 k^{-\frac{\beta}{\beta-1}},$$

for all $k \geq 1$, with some positive constants a_1, a_2, b_1 and b_2. From here we conclude that

$$y_k - y_{k+1} \leq \frac{b_2}{a_1} k^{\frac{\alpha}{\alpha-1} - \frac{\beta}{\beta-1}} (x_k - x_{k+1}) \leq \frac{b_2}{a_1}(x_k - x_{k+1}), \tag{9}$$

for all $k \geq 1$, where in the last inequality we used $\alpha \geq \beta$. From (9) it can be easily seen that

$$y_k - y_{k+l} \leq \frac{b_2}{a_1}(x_k - x_{k+l}), \ k, l \geq 1. \tag{10}$$

We now define the projection $\Psi : S \setminus \{(x_0, y_0)\} \to \mathbb{R}$ onto the x-axis: $\Psi(x, y) = x$. Note that $\Psi(S \setminus \{(x_0, y_0)\}) = A \setminus \{x_0\}$. It is clear that $|\Psi(x_k, y_k) -$

$\Psi(x_{k+l}, y_{k+l})| \leq |x_k - x_{k+l}| + |y_k - y_{k+l}|$ with $k, l \geq 1$. On the other hand, using (10) we get

$$\begin{aligned} |\Psi(x_k, y_k) - \Psi(x_{k+l}, y_{k+l})| &= |x_k - x_{k+l}| \\ &\geq \frac{1}{2}|x_k - x_{k+l}| + \frac{a_1}{2b_2}|y_k - y_{k+l}| \\ &\geq L\,(|x_k - x_{k+l}| + |y_k - y_{k+l}|) \end{aligned}$$

with $k, l \geq 1$ and $L := \min\{\frac{1}{2}, \frac{a_1}{2b_2}\} > 0$. Thus, Ψ is a bi-Lipschitz function and we therefore have $\dim_B(S \setminus \{(x_0, y_0)\}) = \dim_B \Psi(S \setminus \{(x_0, y_0)\})$ (see also Section 1). □

Remark 4. *A similar result can be proved for higher dimensional orbits (in $\mathbb{R}^p$ with a finite p). More precisely, if we assume that $A_i = \{x_k^{(i)}\}_{k\in\mathbb{N}}$ has the properties given in Lemma 2 with $\alpha_i > 1$, for all $i = 1, 2, \ldots, p$, and if $\alpha_{i_0} \geq \alpha_i$ for some i_0 and for all $i = 1, 2, \ldots, p$, then we have $\dim_B S = \dim_B A_{i_0} = 1 - \frac{1}{\alpha_{i_0}}$ where $S = \{(x_k^{(1)}, x_k^{(2)}, \ldots, x_k^{(p)})\}_{k\in\mathbb{N}}$.*

Theorem 2. (**Box dimension near nilpotent singularity**) *Suppose that the origin of (5) has a separatrix and that the orbit $S = \{(x_k, y_k)\}_{k\in\mathbb{N}}$ of (x_0, y_0) on the separatrix, generated by the unit-time map of (5), tends to the origin. Then the box dimension of S, $A = \{x_k\}_{k\in\mathbb{N}}$ and $B = \{y_k\}_{k\in\mathbb{N}}$ exists and it is independent of the initial point (x_0, y_0). Moreover, the values of $\dim_B S$, $\dim_B A$ and $\dim_B B$ are equal to the ones given in Table 1.*

Remark 5. *Before we prove Theorem 2, we would like to stress that the same fractal classification is true for "repelling" separatrices (thus, with the dynamics pointing away from the origin), i.e. for a fixed (m, n) we end up with the same box dimensions of backward orbits on the repelling separatrices (if they exist), like in Table 1. Indeed, if we denote by ϕ_t the flow of (5) and if there exists a repelling separatrix for a fixed (m, n), then the (backward) orbit on the separatrix, with initial point $(x_0, y_0) \neq (0, 0)$ and generated by ϕ_{-1}, is equal to the (forward) orbit with the same initial point and generated by the unit-time map of (5), multiplied by -1. On the other hand, since the vector field (5), multiplied by -1, is not of type (5), we apply the coordinate change $x \to -x$ and get a system of the type (5), with the same (m, n) (a and b may have different sign). The orbit in the new coordinates has the same properties like the old one: it converges to the origin and is located on a separatrix with the same exponent in the leading term. Now, it suffices to apply Theorem 2 to this orbit (note that $x \to -x$ is a bi-Lipschitz function).*

Proof. We assume that the initial point (x_0, y_0) of the orbit S which tends to the origin satisfies $x_0 > 0$ (i.e. the coefficient in front of the leading term of the separatrix is negative). The study of the case where $x_0 < 0$ is analogous. We denote by γ the order of the leading term in the expansion of the separatrices given in Table 1. We have $\gamma \in]1, m[$ for each separatrix. Looking at the x-component of (6), (7) and (8) we have that $x_k - x_{k+1} \simeq x_k^\gamma$ as $k \to \infty$ after substitution $-y_k \simeq x_k^\gamma$ (for each separatrix in Table 1 on which orbits with $x_0 > 0$ tend to the origin). Following [4] we find that $\dim_B A = 1 - \frac{1}{\gamma}$ and it is independent of the initial point x_0. It is clear that $\{x_k\}_{k\in\mathbb{N}}$ satisfies the assumptions of Lemma 2 (the same will be true for $\{y_k\}_{k\in\mathbb{N}}$).

To find $\dim_B B$, we have to distinguish between three cases (see Table 1): Hamiltonian like case, singular like case and mixed case. At $m = 2n+1$, the leading property of the terms x_k^m and $x_k^n y_k$ changes, with $x_k \simeq (-y_k)^{\frac{1}{\gamma}}$ as $k \to \infty$.

Hamiltonian like case ($m < 2n+1$). Here we have $\gamma = \frac{m+1}{2}$. From the y-component of (6), (7) and (8) follows that $(-y_k) - (-y_{k+1}) \simeq (-y_k)^{\frac{m}{\gamma}}$ as $k \to \infty$. Thus, the leading term in this case is x_k^m. Again, [4] implies that $\dim_B B = 1 - \frac{\gamma}{m} = \frac{m-1}{2m}$ and it is independent of $y_0 < 0$. Using Lemma 2 we have $\dim_B S = \dim_B A = \frac{m-1}{m+1}$. Note that $n = \infty$ is also included in this case.

Singular like case ($m > 2n+1$). First, we take $\gamma = n+1$. Using the y-component in (8) we get $(-y_k) - (-y_{k+1}) \simeq (-y_k)^{\frac{n}{\gamma}+1}$ as $k \to \infty$ ($x_k^n y_k$ is the leading term). Thus, $\dim_B B = \frac{n}{2n+1}$ and Lemma 2 gives $\dim_B S = \dim_B A = \frac{n}{n+1}$. This is also true for $m = \infty$.

Now we take $\gamma = m-n$. A separatrix is the graph of $y = f(x) = -\frac{a}{b}x^\gamma + h.o.t.$ with $\frac{a}{b} > 0$. Note that $ax^m + bx^n y \equiv 0$ for $y = -\frac{a}{b}x^\gamma$ and our goal is to find the order l ($> \frac{m}{\gamma}$) of the leading term of the y-component in (5) after the substitution $x = f^{-1}(y)$. Once we have the order l we conclude that $\dim_B B = 1 - \frac{1}{l}$ (see Lemma 3). First, let us assume that the system (5) has the following form: $\{\dot{x} = y, \dot{y} = ax^m + bx^n y\}$. Since the curve $y = f(x)$ is invariant for (5), we easily find that $f(x) = -\frac{a}{b}x^\gamma + \frac{a^2\gamma}{b^3}x^{\gamma+m-2n+1} + h.o.t.$ and therefore

$$f^{-1}(y) = \left(-\frac{b}{a}y\right)^{\frac{1}{m-n}} + \frac{a}{b^2}\left(-\frac{b}{a}y\right)^{\frac{m-2n}{m-n}} + h.o.t.$$

Using this we obtain the dynamics of (5) along the curve $y = f(x)$ expressed in terms of y:

$$\dot{y} = \frac{a^2(m-n)}{b^2}\left(-\frac{b}{a}y\right)^{\frac{2m-2n-1}{m-n}} + h.o.t.$$

Thus, $l = \frac{2m-2n-1}{m-n}$ and $\dim_B B = \frac{m-n-1}{2m-2n-1}$. If we deal with the general system (5), we end up with the same conclusion. Indeed, if we denote the y-component in (5) by $X_2(x,y)$, then the invariant curve $y = f(x)$ satisfies

$$X_2(x, f(x)) = f'(x)f(x).$$

Thus, $X_2(x, f(x))$ is of order $2m-2n-1$ because f is of order $m-n$. Now, since f^{-1} is of order $\frac{1}{m-n}$, we have that $X_2(f^{-1}(y), y)$ is of order $l = \frac{2m-2n-1}{m-n}$ (in $-y$). The positive coefficient in front of $(-y)^l$ is as above equal to $(m-n)(\frac{a}{b})^{\frac{1}{m-n}}$. This completes the proof in the singular like case.

Mixed case ($m = 2n+1$). Here we have $\gamma = n+1$. Using (8) we get $(-y_k) - (-y_{k+1}) \simeq (-y_k)^{\frac{2n+1}{n+1}}$ as $k \to \infty$. Indeed, it suffices to notice that for $y = \frac{b \pm \sqrt{\Delta}}{2(n+1)}x^{n+1}$ we have that

$$ax^m + bx^n y = \frac{b^2 \pm b\sqrt{\Delta} + 2a(n+1)}{2(n+1)}x^{2n+1}$$

with $b^2 \pm b\sqrt{\Delta} + 2a(n+1) \neq 0$. Thus, $\dim_B B = \frac{n}{2n+1}$ and $\dim_B S = \dim_B A = \frac{n}{n+1}$. □

Lemma 3. *Consider a one-dimensional equation* $\dot{x} = \alpha x^{\epsilon p}(1 + g(x^{\epsilon}))$*, where* $\alpha < 0$*,* $\epsilon > 0$*,* $\epsilon p > 1$ *and* g *is a* C^1*- function including in* 0 *with* $g(0) = 0$*. Then* $\dim_B A = 1 - \frac{1}{\epsilon p}$ *where* A *is the orbit of* $x_0 > 0$ *and* $x_0 \sim 0$ *generated by the unit-time map of the equation.*

Proof. Since the system is C^1, the existence and uniqueness of solutions and continuity with respect to initial conditions imply that the (unique) solution $\psi(t, x_0)$, with $\psi(0, x_0) = x_0$, is a map of class C^1. For any small $x_0 \geq 0$ and $t \geq 0$ kept in a compact set we have

$$\psi(t, x_0) = x_0 + \alpha \int_0^t \psi(s, x_0)^{\epsilon p}(1 + g(\psi(s, x_0)^{\epsilon}))\, ds. \tag{11}$$

Since $x = 0$ is a singularity of the differential equation, we have $\psi(s, 0) \equiv 0$, i.e. $\psi(s, x_0) = O(x_0)$. From (11) follows that $\psi(t, x_0) = x_0 + O(x_0^{\epsilon p})$. Substituting this for $\psi(s, x_0)$ in (11) and taking $t = 1$ we get $x_0 - \psi(1, x_0) \simeq x_0^{\epsilon p}$ as $x_0 \to 0$ (note that $\alpha < 0$). Following Theorem 1 from [4] we now obtain that $\dim_B A = 1 - \frac{1}{\epsilon p}$ because $\epsilon p > 1$. □

In the proof of Theorem 2 in the singular case we used Lemma 3 where $\epsilon = \frac{1}{m-n}$, $p = 2m - 2n - 1$ and g is C^r with $r \in \mathbb{N}$ as large as we need using the center manifold theorem (we also used the fact that $y \mapsto -y$ is a bi-Lipschitz function).

3 Nilpotent focus

In this section we obtain the connection between the box dimension of an orbit of the Poincaré map and the cyclicity of nilpotent focus. We use Theorem 1.7 from [6] and results from [7]. First, we recall Theorem 1.7 in [6] which gives an upper bound for the cyclicity of the nilpotent focus.

We study small limit cycles near the origin in an analytic δ-family of planar systems

$$\begin{aligned} \dot{x} &= y + X(x, y, \delta) \\ \dot{y} &= Y(x, y, \delta) \end{aligned} \tag{12}$$

with $\delta = (\delta_1, \delta_2, \ldots, \delta_l) \in D \subset \mathbb{R}^l$ where D is a simply connected domain and $X, Y = \mathcal{O}(|x, y|^2)$ for all $\delta \in D$. Let $y = f(x, \delta)$ be the characteristic curve of (12) and define $F(x, \delta) = -Y(x, f(x, \delta), \delta)$ and $G(x, \delta) = -(\frac{\partial X}{\partial x} + \frac{\partial Y}{\partial y})(x, f(x, \delta), \delta)$. We make the following assumptions about the functions F and G for all $\delta \in D$:

$$\begin{aligned} F(x, \delta) &= \sum_{j \geq 2n-1} a_j(\delta) x^j, \;\; n \geq 2, \;\; a_{2n-1}(\delta) > 0, \text{ and} \\ G(x, \delta) &= \sum_{j \geq n-1} b_j(\delta) x^j, \;\; b_{n-1}^2(\delta) - 4n a_{2n-1}(\delta) < 0. \end{aligned} \tag{13}$$

Theorem 1 (see (3)(i) and (4)(iii1)) implies now that the system (12) has a center or a focus at the origin for all $\delta \in D$. The origin is thus a m-multiple singular point with $m = 2n - 1$ for all $\delta \in D$. Further, we define a Poincaré map of the

system (12) on the characteristic curve $y = f(x, \delta)$. For each $\delta \in D$ and $x_0 \neq 0$, $|x_0|$ small, consider the solution $(x(t, x_0, \delta), y(t, x_0, \delta))$ of the system (12) with the initial condition $(x(0), y(0)) = (x_0, f(x_0, \delta))$. Then there exists the unique least positive number $\tau = \tau(x_0, \delta) > 0$ such that $y(\tau, x_0, \delta) = f(x(\tau, x_0, \delta), \delta)$ and $x_0 x(\tau, x_0, \delta) > 0$. We define the Poincaré map: $P(x_0, \delta) := x(\tau, x_0, \delta)$, $x_0 \neq 0$ and $P(0, \delta) = 0$. It should be clear that P is continuous in $x_0 = 0$. By Theorem 1.5 from [6] we have that there is an analytic function $\bar{P}(x_0, \delta)$ in $x_0 = 0$ such that the partial derivative of $\bar{P}$ w.r.t. x_0 in $(0, \delta)$ is positive,

$$\bar{P}(x_0, \delta) = x_0 + \sum_{j \geq 1} v_j(\delta) x_0^j$$

for $|x_0|$ sufficiently small and such that $P(x_0, \delta) = \bar{P}(x_0, \delta)$ for all $x_0 \geq 0$ small (this equality is true for all $|x_0|$ small if n is odd). For more details see [6].

Theorem 3. ([6], Theorem 1.7) *Let system* (12) *satisfy the conditions* (13) *for all* $\delta \in D$. *Write* $p_n = (1 + (-1)^n)/2$.

(1) If there is an integer $k \geq 1$ *such that*

$$\sum_{j=1}^{k+1} |v_{2j-1+p_n}| > 0, \ \ \forall \delta \in D,$$

then there exists a neighborhood $\mathcal{U}$ *of the origin such that the system (*12*) has at most* k *limit cycles in* $\mathcal{U}$ *for all* $\delta \in \bar{D}$, *where* $\bar{D}$ *is any compact subset of* D.

(2) If there is $\delta_0 \in D$ *such that* $v_{2k+1+p_n}(\delta_0) \neq 0$, *then for all* $\delta \in D$ *near* δ_0 *system (*12*) has at most* k *limit cycles in a neighborhood of the origin.*

Now we are able to state and prove the main result of this section.

Theorem 4. (**Cyclicity of nilpotent focus and box dimension**) *Let system* (12) *satisfy the conditions* (13) *for all* $\delta \in D$. *Let* $\Gamma(\delta_0)$ *be a spiral trajectory of (*12*) near the origin for some* $\delta_0 \in D$. *Let* $P(x, \delta_0)$ *be the Poincaré map of (*12*) with* $\delta = \delta_0$ *on the characteristic curve* $y = f(x, \delta_0)$. *Suppose that the sequence* $S(x_1) = (x_i)_{i \geq 1}$ *defined by* $x_{i+1} = P(x_i, \delta_0)$ *(a stable focus) or* $x_{i+1} = P^{-1}(x_i, \delta_0)$*(an unstable focus), with* $x_1 > 0$ *small and fixed, has the box dimension equal to* $1 - \frac{1}{2k+1}$ *with* n *odd or* $1 - \frac{1}{2k+2}$ *with* n *even where* $k \geq 1$ *is an integer. Then for all* $\delta \in D$ *near* δ_0 *the system (*12*) has at most* k *limit cycles in a* δ*-uniform neighborhood of the origin.*

Proof. We know that in both cases (n odd and even) the Poincaré map $P(x, \delta_0)$ is equal to $\bar{P}(x, \delta_0)$ for $x \geq 0$ where $\bar{P}(x, \delta_0)$ is analytic in $x = 0$. Since $\dim_B S(x_1) > 0$, then we know that $x = 0$ is a nonhyperbolic fixed point of $\bar{P}$ and $\bar{P}'(0) = 1$ (see e.g. [7]). When $\dim_B S(x_1) = 1 - \frac{1}{2k+1}$ (resp. $\dim_B S(x_1) = 1 - \frac{1}{2k+2}$), then we have $\bar{P}(x, \delta_0) = x + v_{2k+1}(\delta_0) x^{2k+1} + \mathcal{O}(x^{2k+2})$ with $v_{2k+1}(\delta_0) \neq 0$ (resp. $\bar{P}(x, \delta_0) = x + v_{2k+2}(\delta_0) x^{2k+2} + \mathcal{O}(x^{2k+3})$ with $v_{2k+2}(\delta_0) \neq 0$). This follows from Theorem 6 in [7]. In both cases we have thus $v_{2k+1+p_n}(\delta_0) \neq 0$. The statement follows now from Theorem 3(2). □

Remark 6. *We attempted to numerically verify the box dimension results from Theorem 4 in the same sense as done for Theorem 2, see Section 5. Unfortunately, numerical calculation of sequence* S *from Theorem 4 involving Poincaré*

map is very slow, so we were unable to produce enough elements of the sequence S to be able to numerically reliably calculate the box dimension of S in any reasonable time and even on simplest systems (12). The convergence of numerical methods (15), (16) and (17) for estimating the box dimension of a given sequence is very slow. We hope further research might solve this issues.

4 Fractal analysis of Bogdanov-Takens bifurcations

In this section we give a fractal analysis of singularities in Bogdanov-Takens bifurcations, using Theorem 2 and the results obtained in [7, 8, 22]. The box dimension jumps as we vary bifurcation parameters. It suffices to deal with the following normal form for the Bogdanov-Takens bifurcations:

$$\begin{aligned} \dot{x} &= y \\ \dot{y} &= \beta_1 + \beta_2 x + x^2 - xy, \end{aligned} \tag{14}$$

where $\beta_{1,2} \in \mathbb{R}$ are the bifurcation parameters. The bifurcation diagram of the Bogdanov-Takens bifurcations is given in Figure 2 (for more details see [11]). We

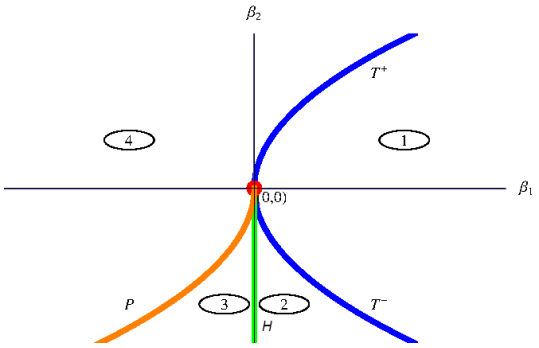

Figure 2: Bifurcation diagram of Bogdanov-Takens bifurcations.

denote by H the negative part of the β_2-axis and it represents the curve along which a Hopf bifurcation occurs. For $\beta_1 = \beta_2 = 0$ we have a cusp at the origin and we get $\dim_B S = \dim_B A = 1/3$ and $\dim_B B = 1/4$ on the separatrices (see Theorem 2 or Table 1). For other (β_1, β_2)-values we use the results from [7, 8, 22]. In region 1 there are no singularities. By passing through the curve T^- a saddle and a node appear, so it is a saddle-node bifurcation curve. On a center manifold of the saddle-node singularity we have $\dim_B S = \dim_B A = 1/2$ and $\dim_B B = 0$ (see Figure 3 and [7, 8]). In the region 2 the node becomes a focus, and crossing the curve H a limit cycle is born. The box dimension of spiral trajectories along the Hopf bifurcation curve is $4/3$ (see Figure 4 and [22]). Passing through the curve P a saddle homoclinic bifurcation occurs, i.e. a saddle-loop appears. In region 4 the saddle-loop is broken and there are two singularities, a saddle and a node. If we continue the journey clockwise and finally return to region 1, the saddle-node bifurcation occurs once more (see

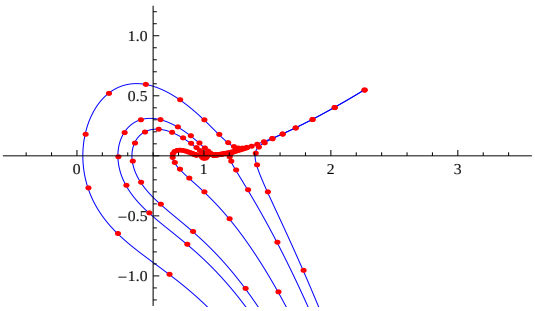

Figure 3: Curve T^-, $\dim_B S = 1/2$ for discrete orbit generated by the unit-time map on a center manifold of the saddle-node singularity.

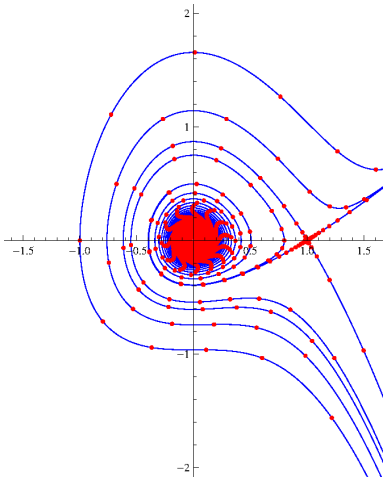

Figure 4: Curve H, $\dim_B S = 4/3$ for spiral trajectory.

Figure 5). All such objects are unfolded in the cusp with $\dim_B S = 1/3$, for $\beta_1 = \beta_2 = 0$. Notice that the box dimension is nontrivial when some local bifurcation occurs. All hyperbolic singularities inside the regions have trivial box dimensions. By the above analysis of the Bogdanov-Takens bifurcations we show how box dimensions of the unit-time map are connected to the appropriate bifurcations of continuous systems.

5 Numerical verification of box dimensions in Table 1

This section is dedicated to the numerical calculation of the box dimensions given in Table 1. In each case, we choose a system and numerically calculate the vector $(\dim_B S, \dim_B A, \dim_B B)$, which is attached to the separatrices of this system. In the Hamiltonian case (resp. the singular case and the mixed case) we take a cusp (resp. saddle-node and saddle). Of course, a similar

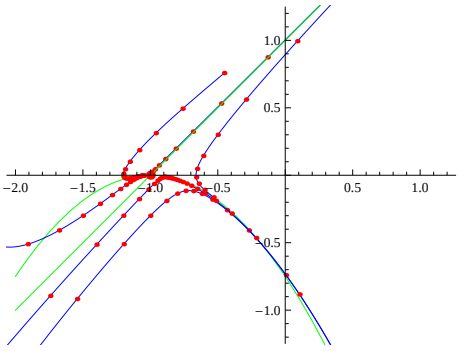

Figure 5: Curve T^+, $\dim_B S = 1/2$ for discrete orbit generated by the unit-time map on a center manifold.

numerical analysis could be performed for other phase portraits in Table 1.

To find $\dim_B A$ and $\dim_B B$, one has to develop numerical methods for calculating the box dimension of one-dimensional (convergent and decreasing) sequences. This was done in [1, 9, 10], where the cyclicity and bifurcations of canard cycles in two-dimensional slow-fast systems were investigated using a so-called box dimension approach (see Proposition 1 in Section 5.1). To estimate $\dim_B S$ (S is a two-dimensional orbit), we use the decomposition of S into tail and nucleus (see e.g. [18]) and find two formulas for a numerical calculation of $\dim_B S$, see Section 5.2. In Section 5.3 we estimate the box dimensions.

5.1 The box dimension of one-dimensional orbits

In the one-dimensional ambient space we have

Proposition 1. *Let $A = \{x_k\}_{k\in\mathbb{N}}$ be a decreasing sequence which tends to 0 with an initial point x_0 such that $x_k - x_{k+1} \simeq x_k^\alpha$ as $k \to \infty$, for $\alpha > 1$, and such that $(x_k - x_{k+1})_{k\in\mathbb{N}}$ is monotonically nonincreasing. Then $\dim_B A = \frac{\alpha-1}{\alpha}$ and we have that*

$$\dim_B A = \lim_{k\to\infty} \frac{\ln k}{-\ln(x_k - x_{k+1})}, \tag{15}$$

$$\dim_B A = \lim_{k\to\infty} \frac{1}{1 - \frac{\ln x_k}{\ln k}} \tag{16}$$

and

$$\dim_B A = \lim_{k\to\infty} \Big(1 - \frac{\ln\big(k(x_k - x_{k+1}) + x_k\big)}{\ln\big(\frac{x_k - x_{k+1}}{2}\big)}\Big). \tag{17}$$

Remark 7. *Proposition 1 has been proved in [1]. The proof of Proposition 1 is based on Theorem 1 in [4] which implies that $\dim_B A = \frac{\alpha-1}{\alpha}$ and $x_k \simeq k^{-\frac{1}{\alpha-1}}$ as $k \to \infty$. Now, it can be easily seen that (15), (16) and (17) hold for $\alpha > 1$.*

Remark 8. *A motivation for the formulas given in (15), (16) and (17) comes from Section 3.4 in [18] where similar expressions have been used to (numerically) compute the box dimension of the Cantor set. In (15) we deal with a Cahen-type formula while (16) is related to the Borel rarefaction index of A.*

The formula in (17) follows from the decomposition of A into tail and nucleus (see [18]).

5.2 The box dimension of two-dimensional orbits

To numerically estimate $\dim_B S$ of a planar two-dimensional orbit S from Theorem 2, we use the decomposition of S into tail and nucleus, like in (17). We work with the following equivalent definition of the box dimension (see [5]):

$$\underline{\dim}_B S = \liminf_{\epsilon\to 0^+}\left(2-\frac{\ln|S_\epsilon|}{\ln\epsilon}\right),\quad \overline{\dim}_B S = \limsup_{\epsilon\to 0^+}\left(2-\frac{\ln|S_\epsilon|}{\ln\epsilon}\right). \tag{18}$$

We first define

$$\epsilon_k = \frac{\sqrt{(x_k-x_{k+1})^2+(y_k-y_{k+1})^2}}{2}. \tag{19}$$

Since S satisfies the assumptions in Lemma 2, we have that $\epsilon_k \to 0$ monotonically. Contrary to the one-dimensional case, here it is not possible to get the exact formula for the area of ϵ_k-neighborhood $|S_{\epsilon_k}|$. Nonetheless reasonably close lower and upper bounds are possible. Since $\{x_k\}_{k\in\mathbb{N}}$, $\{y_k\}_{k\in\mathbb{N}}$ and $\{\epsilon_k\}_{k\in\mathbb{N}}$ are monotonically nonincreasing sequences tending to 0, a simple separation between the tail and the nucleus part of S_{ϵ_k} is possible, see [18]. By S_{t,ϵ_k} we denote the ϵ_k-neighborhood of the tail and by S_{n,ϵ_k} the ϵ_k-neighborhood of the nucleus. From $S_{\epsilon_k} = S_{t,\epsilon_k}\cup S_{n,\epsilon_k}$ and $S_{t,\epsilon_k}\cap S_{n,\epsilon_k}=\emptyset$ follows that $|S_{\epsilon_k}| = |S_{t,\epsilon_k}| + |S_{n,\epsilon_k}|$. As the length of the part of the separatrix from point (x_{k+1}, y_{k+1}) to the origin is less or equal to $x_{k+1}+y_{k+1}$, it is easy to see that

$$|S_{t,\epsilon_k}| = k\cdot\epsilon_k^2\pi,\quad \epsilon_k^2\pi < |S_{n,\epsilon_k}| < 2\epsilon_k(x_{k+1}+y_{k+1})+\epsilon_k^2\pi.$$

It follows that

$$(k+1)\epsilon_k^2\pi < |S_{\epsilon_k}| < 2\epsilon_k(x_{k+1}+y_{k+1})+(k+1)\epsilon_k^2\pi. \tag{20}$$

Finally, substituting (20) in (18) and using the fact that $\dim_B S$ exists (see Lemma 2) we get the lower bound on $\underline{\dim}_B S$ and the upper bound on $\overline{\dim}_B S$,

$$\underline{\dim}_B S \;\geq\; \lim_{k\to\infty}\left(2-\frac{\ln\left((k+1)\epsilon_k^2\pi\right)}{\ln\epsilon_k}\right), \tag{21}$$

$$\overline{\dim}_B S \;\leq\; \lim_{k\to\infty}\left(2-\frac{\ln\left(2\epsilon_k(x_{k+1}+y_{k+1})+(k+1)\epsilon_k^2\pi\right)}{\ln\epsilon_k}\right). \tag{22}$$

Using the assumptions in Lemma 2, (19) and the property of x_k and y_k as $k\to\infty$ from Remark 7, it can be easily seen that the limits in (21) and (22) exist and have the same value ($1-\frac{1}{\alpha}$ if $\alpha\geq\beta$ and $1-\frac{1}{\beta}$ if $\alpha<\beta$). This implies

Proposition 2. *Let $S=\{(x_k,y_k)\}_{k\in\mathbb{N}}$ satisfy the assumptions in Lemma 2. Then we have*

$$\dim_B S = \lim_{k\to\infty}\left(2-\frac{\ln\left((k+1)\epsilon_k^2\pi\right)}{\ln\epsilon_k}\right) \tag{23}$$

and

$$\dim_B S = \lim_{k\to\infty}\left(2-\frac{\ln\left(2\epsilon_k(x_{k+1}+y_{k+1})+(k+1)\epsilon_k^2\pi\right)}{\ln\epsilon_k}\right). \tag{24}$$

Remark 9. *The box dimension of S is trivially bounded by the same limits in (21) and (22).*

Similar two-dimensional generalizations are not possible for methods (15) and (16), so for the estimation of the box dimension of a two-dimensional sequence we use only our generalization of (17).

5.3 The estimation of the box dimensions

The goal of this section is to numerically compute the relevant box dimensions for the cusp in Hamiltonian case, the saddle-node in singular case and the saddle in mixed case (see Tables 2 and 3). This provides a numerical validation of results from Theorem 2, given in Table 1.

5.3.1 The Hamiltonian case (cusp)

We proceed by setting $\beta_1 = \beta_2 = 0$ in (14) and get the system

$$\begin{aligned} \dot{x} &= y \\ \dot{y} &= x^2 - xy. \end{aligned} \tag{25}$$

The first step is to numerically solve the system (25) for the initial condition (x_0, y_0) taken on the separatrix

$$y = -\sqrt{\frac{2}{3}} x^{\frac{3}{2}} + \cdots, x > 0,$$

tending to the origin and given in Table 1. By numerically solving the system (25) we mean computing a finite number K of elements in the orbit $S = \{(x_k, y_k)\}_{k\in\mathbb{N}}$ generated by the unit-time map of (25), which we denote by $S' = \{(x_k, y_k)\}_{1\leq k\leq K}$. We numerically estimate box dimensions $\dim_B A$ and $\dim_B B$ of $A = \{x_k\}_{k\in\mathbb{N}}$ and $B = \{y_k\}_{k\in\mathbb{N}}$ from Theorem 2 using formulas (15), (16) and (17) in Proposition 1. We also estimate $\dim_B S$ from Theorem 2 using formulas (23) and (24) in Proposition 2.

5.3.2 The singular case (saddle-node)

Here we take $n = 1$, $m = 4$, $a = 1$ and $b = 1$ in (5) and get the system

$$\begin{aligned} \dot{x} &= y \\ \dot{y} &= x^4 + xy, \end{aligned} \tag{26}$$

which is solved numerically in the same sense as the system (25). The initial condition is taken on a separatrix $y = \frac{1}{2}x^2 + \cdots$ or $y = -x^3 + \cdots$, given in Table 1. As before, box dimensions $\dim_B A$, $\dim_B B$ and $\dim_B S$ from Theorem 2 are estimated.

5.3.3 The mixed case (saddle)

Similarly as in the previous section, we take $n = 1$, $m = 2n + 1 = 3$, $a = 1$ and $b = 1$ in (5) and solve numerically the resulting system

$$\begin{aligned} \dot{x} &= y \\ \dot{y} &= x^3 + xy, \end{aligned} \tag{27}$$

as before. Again, we take the initial condition on the separatrix $y = x^2 + \cdots$ from Table 1 and estimate $\dim_B A$, $\dim_B B$ and $\dim_B S$.

5.3.4 Implementation details

All numerical calculations are implemented using Wolfram Mathematica 12.0. See `https://github.com/FRABDYN/NilpotentSingularities` where our code is available for download. We use the automatic numerical precision control mechanisms, built in Mathematica software, so all numerical calculations can be regarded as interval calculations. For numerically solving system (25) we use Mathematica "NDSolve" function together with an increased numerical precision above the standard floating point machine precision.

The precision in Mathematica is the effective number of digits of precision of the number x considered, given by expression $-\log_{10}(e/x)$, where e is the absolute uncertainty in x. The precision is increased to 75 decimal places, which is carefully chosen as a compromise between the computation runtime and the final precision in the numerically estimated box dimension. More precisely, Mathematica function "NDSolve" is used to produce a numerical solution that is guaranteed to be correct to at least 75 decimal places.

An increased precision is essential for our calculations where we managed to use values of K over 10^{65} for all cases except for separatrix $y = -x^3 + \cdots$ from the singular case. For such big K, values x_K and x_{K-1}, and also values y_K and y_{K-1}, are very close. For instance in expression (19) the precision is reduced to less than 10 decimal places, which happens because of the subtraction of close numbers represented with finite decimal places in the computer. For separatrix $y = -x^3 + \cdots$ from the singular case due to slow convergence we used much smaller $K \approx 5 \cdot 10^9$, where precision of only 20 decimal places is sufficient.

Notice that we don't have to explicitly compute all elements in finite orbit S', which would actually not be possible. What we do is explicitly compute numerical solution of systems (25), (26) and (27) in terms of Mathematicas "InterpolatingFunction" object, which is a piecewise polynomial interpolation that guaranties the sought numerical precision. Then we evaluate this piecewise polynomial, for integer values of time K and $K-1$, effectively getting points (x_K, y_K) and (x_{K-1}, y_{K-1}) from orbit S. Only these two points, together with K, are used to estimate the limit in formulas (15), (16), (17), (21), (22).

Another numerical finesse is to compute finite orbit S' in the reversed direction, that is, to start numerical system integration for an initial condition near the origin and to reverse the direction of the orbit on a separatrix so that it tends away of the origin. This is achieved by multiplying the right hand side of systems (25), (26) and (27) by a constant -1, which is equivalent to reversing the direction of time in the system integration, see Remark 5. The system integration is stopped when the orbit exits the circle of radius 1. The advantage of this approach with reversed orbit computation is that we achieve much greater numerical stability of "NDSolve". This detail proved to be crucial for an efficient numerical solution.

5.3.5 Numerical results

Numerical results are given in Table 2 and consist of a numerical estimation of $\dim_B A$ and $\dim_B B$, using all three methods (15), (16) and (17) from Proposition 1. Also, in Table 3, a numerical estimation of the box dimension $\dim_B S$ is given, using the two methods from Proposition 2. Results are given for all three considered cases. Note that the separatrix $y = -x^3 + \cdots$ from the singular case produces the biggest error due to the slow convergence of associated orbits (as explained in Section 2.1, the separatrix comes from a center direction where the hyperbolicity is lost).

			Numerical estimates using method		
System and separatrix	Box dim.	Theory value	(15)	(16)	(17)
cusp (25), $y = -\sqrt{\frac{2}{3}}x^{\frac{3}{2}} + \cdots$	$\dim_B A$	1/3	0.335177	0.334661	0.337103
	$\dim_B B$	1/4	0.251496	0.251036	0.252842
saddle-node (26), $y = \frac{1}{2}x^2 + \cdots$	$\dim_B A$	1/2	0.501155	0.501155	0.504610
	$\dim_B B$	1/3	0.334361	0.333846	0.336286
saddle-node (26), $y = -x^3 + \cdots$	$\dim_B A$	2/3	0.646604	0.659842	0.684735
	$\dim_B B$	2/5	0.325211	0.392689	0.502074
saddle (27), $y = x^2 + \cdots$	$\dim_B A$	1/2	0.500000	0.500000	0.503449
	$\dim_B B$	1/3	0.333846	0.333333	0.335769

Table 2: Numerically computed estimates for box dimensions $\dim_B A$ and $\dim_B B$, using all three methods from Proposition 1.

			Num. est. using (21) and (22)	
System and separatrix	Box dim.	Theory value	Lower estimate	Upper estimate
cusp (25), $y = -\sqrt{\frac{2}{3}}x^{\frac{3}{2}} + \cdots$	$\dim_B S$	1/3	0.337205	0.338300
saddle-node (26), $y = \frac{1}{2}x^2 + \cdots$	$\dim_B S$	1/2	0.503807	0.506537
saddle-node (26), $y = -x^3 + \cdots$	$\dim_B S$	2/3	0.666374	0.702302
saddle (27), $y = x^2 + \cdots$	$\dim_B S$	1/2	0.502648	0.505373

Table 3: Numerically computed estimates for box dimension $\dim_B S$ using the methods from Proposition 2.

Acknowledgement. This research was supported by: Croatian Science Foundation (HRZZ) grant PZS-2019-02-3055 from Research Cooperability program funded by the European Social Fund.

References

[1] V. Crnković, R. Huzak, and D. Vlah. Fractal dimensions and two-dimensional slow-fast systems (submitted). 2020.

[2] F. Dumortier, J. Llibre, and J. Artés. *Qualitative theory of planar differential systems.* Universitext. Springer-Verlag, Berlin, 2006.

[3] F. Dumortier, P. R. Rodrigues, and R. Roussarie. *Germs of diffeomorphisms in the plane*, volume 902 of *Lecture Notes in Mathematics*. Springer-Verlag, Berlin-New York, 1981.

[4] N. Elezović, V. Županović, and D. Žubrinić. Box dimension of trajectories of some discrete dynamical systems. *Chaos Solitons Fractals*, 34(2):244–252, 2007.

[5] K. Falconer. *Fractal geometry*. John Wiley and Sons, Ltd., Chichester, 1990. Mathematical foundations and applications.

[6] M. Han and V. G. Romanovski. Limit cycle bifurcations from a nilpotent focus or center of planar systems. *Abstr. Appl. Anal.*, pages Art. ID 720830, 28, 2012.

[7] L. Horvat Dmitrović. Box dimension and bifurcations of one-dimensional discrete dynamical systems. *Discrete Contin. Dyn. Syst.*, 32(4):1287–1307, 2012.

[8] L. Horvat Dmitrović. Box dimension of Neimark-Sacker bifurcation. *J. Difference Equ. Appl.*, 20(7):1033–1054, 2014.

[9] R. Huzak. Box dimension and cyclicity of canard cycles. *Qual. Theory Dyn. Syst.*, 17(2):475–493, 2018.

[10] R. Huzak and D. Vlah. Fractal analysis of canard cycles with two breaking parameters and applications. *Commun. Pure Appl. Anal.*, 18(2):959–975, 2019.

[11] Y. A. Kuznetsov. *Elements of applied bifurcation theory*, volume 112 of *Applied Mathematical Sciences*. Springer-Verlag, New York, second edition, 1998.

[12] Y. Liu and J. Li. New study on the center problem and bifurcations of limit cycles for the Lyapunov system. I. *Internat. J. Bifur. Chaos Appl. Sci. Engrg.*, 19(11):3791–3801, 2009.

[13] P. Mardešić, M. Resman, and V. Županović. Multiplicity of fixed points and growth of ε-neighborhoods of orbits. *J. Differential Equations*, 253(8):2493–2514, 2012.

[14] P. Mardešić, M. Resman, J.-P. Rolin, and V. Županović. Normal forms and embeddings for power-log transseries. *Adv. Math.*, 303:888–953, 2016.

[15] M. Resman. ϵ-neighborhoods of orbits and formal classification of parabolic diffeomorphisms. *Discrete Contin. Dyn. Syst.*, 33(8):3767–3790, 2013.

[16] M. Resman. ϵ-neighbourhoods of orbits of parabolic diffeomorphisms and cohomological equations. *Nonlinearity*, 27(12):3005–3029, 2014.

[17] E. Strozyna and H. Zoladek. The analytic and formal normal form for the nilpotent singularity. *J. Differential Equations*, 179(2):479–537, 2002.

[18] C. Tricot. *Curves and fractal dimension*. Springer-Verlag, New York, 1995. With a foreword by Michel Mendès France, Translated from the 1993 French original.

[19] D. Žubrinić. Analysis of Minkowski contents of fractal sets and applications. *Real Anal. Exchange*, 31(2):315–354, 2005/06.

[20] D. Žubrinić and V. Županović. Fractal analysis of spiral trajectories of some planar vector fields. *Bull. Sci. Math.*, 129(6):457–485, 2005.

[21] D. Žubrinić and V. Županović. Fractal dimensions in dynamics. *Encyclopedia of Math. Physics*, 2:394–402, 2006.

[22] D. Žubrinić and V. Županović. Poincaré map in fractal analysis of spiral trajectories of planar vector fields. *Bull. Belg. Math. Soc. Simon Stevin*, 15(5, Dynamics in perturbations):947–960, 2008.